Publ. Astron. Soc. Japan (2014) 66 (2), 37 (1–10)
doi: 10.1093/pasj/psu019

X-ray development of the classical nova V2672 Ophiuchi with Suzaku

Dai TAKEI,[1,2,*] Masahiro TSUJIMOTO,[3] Jeremy J. DRAKE,[2] and Shunji KITAMOTO[4]

[1]Institute of Physical and Chemical Research (RIKEN), RIKEN SPring-8 Center, 1-1-1 Kouto, Sayo, Hyogo 679-5148
[2]Smithsonian Astrophysical Observatory (SAO), 60 Garden Street, Cambridge, MA 02138, USA
[3]Japan Aerospace Exploration Agency (JAXA), Institute of Space and Astronautical Science (ISAS), 3-1-1 Yoshino-dai, Chuo-ku, Sagamihara 252-5210
[4]Department of Physics, Rikkyo University, 3-34-1 Nishi-Ikebukuro, Toshima, Tokyo 171-8501

*E-mail: takei@spring8.or.jp

Received 2013 July 10; Accepted 2013 November 21

Abstract

We report on the Suzaku detection of a rapid flare-like X-ray flux amplification early in the development of the classical nova V2672 Ophiuchi. Two target-of-opportunity ~ 25 ks X-ray observations were made 12 and 22 d after the outburst. The flux amplification was found in the latter half of day 12. Time-sliced spectra are characterized by a growing supersoft excess with edge-like structures and a relatively stable optically-thin thermal component with Kα emission lines from highly ionized Si. The observed spectral evolution is consistent with a model that has a time development of circumstellar absorption, for which we obtained a decline rate of $\sim 10\%$–40% on a time scale of 0.2 d on day 12. Such a rapid drop of absorption and short-term flux variability on day 12 suggests inhomogeneous ejecta with dense blobs/holes in the line-of-sight. Then on day 22 the fluxes of both supersoft and thin-thermal plasma components became significantly fainter. Based on the serendipitous results we discuss the nature of this source in the context of both short- and long-term X-ray behavior.

Key words: stars: individual (Nova Ophiuchi 2009, V2672 Ophiuchi) — stars: novae, cataclysmic variables — X-rays: stars

1 Introduction

Classical novae are violent stellar explosions in close binaries that contain a white-dwarf primary accreting material from a red dwarf or giant secondary. Sudden hydrogen fusion is triggered by a thermonuclear runaway in the accreted gas when it exceeds a critical limit (Starrfield et al. 2008). The general picture of nova evolution is characterized by the development of photospheric emission that dominates first in the optical, and then in supersoft X-rays ($\lesssim 1$ keV) as the surrounding ejecta become less opaque. For detailed reviews of novae see e.g., Warner (2003) and Bode and Evans (2008).

The spectral transition from optical to supersoft X-rays is not always as smooth as the simple generalized picture predicts. X-ray snapshots with Swift (e.g., Schwarz et al. 2011) have discovered large and rapid amplitude variability, particularly early in the development of the transition: e.g., in RS Oph 2006 (Osborne et al. 2011), V458 Vul

(Ness et al. 2009a), Nova LMC 2009a (Bode et al. 2009), and KT Eri (Beardmore et al. 2010a). Short-term changes in supersoft X-ray emission can potentially provide valuable insights into the structure and nature of the emitting region, and the spectral development of the source must also play a key part in the physical interpretation.

The mechanism underlying short-term changes in nova outburst X-ray fluxes is still not understood, and neither is it known whether similar physical processes are at work in different systems. Drake et al. (2003) observed a short 15 min X-ray burst from V1494 Aql during the supersoft source phase, which remains unexplained. Ness et al. (2003) suggested that white-dwarf spin is related to the 22 min oscillations seen in V4743 Sgr. Osborne et al. (2011) suggested absorption due to clumpy ejecta for the large flickering of RS Oph 2006. Beardmore et al. (2010b) found a binary period with a 1.77 d modulation in CSS 081007:030559+054715. Ness et al. (2012) argued that reforming accretion blobs caused a flux instability in U Sco 2010. The present set of observations are still sparse, and further progress in this direction demands additional X-ray observations. Since they are currently difficult to predict, progress is likely to come from capturing short-term transient phenomena serendipitously.

The purpose of this paper is to report on the Suzaku detection of a rapid flare-like X-ray flux amplification early in the development of the classical nova V2672 Ophiuchi (V2672 Oph). This represents a rare addition to the currently very small sample of rapid X-ray flux change on short timescales for classical novae, and the advent of time-sliced X-ray spectroscopy provides a unique opportunity to investigate its behavior in detail.

The plan of this paper is as follows: In section 2 we summarize previous studies of this target. In section 3 we introduce our target-of-opportunity observations obtained with the Suzaku satellite. In section 4 we describe the analysis and results. In section 5 we discuss the results in the context of the nature of the source, and a summary is presented in section 6.

2 Target (V2672 Ophiuchi)

2.1 Ground-based observations

An optical nova was discovered on 2009 August 16.515 UT (modified Julian date 55059.52 d) in the constellation Ophiuchus at (RA, Dec) = ($17^{\rm h}38^{\rm m}19\overset{\rm s}{.}68$, $-26^\circ44'14\overset{''}{.}0$) in the equinox J2000.0 (Nakano et al. 2009a). Throughout this paper we define the epoch of the discovery as the origin of time. The nova event showed a visual magnitude of 10.0 mag at discovery in unfiltered CCD camera photometry (Nakano et al. 2009a). Nothing brighter than an

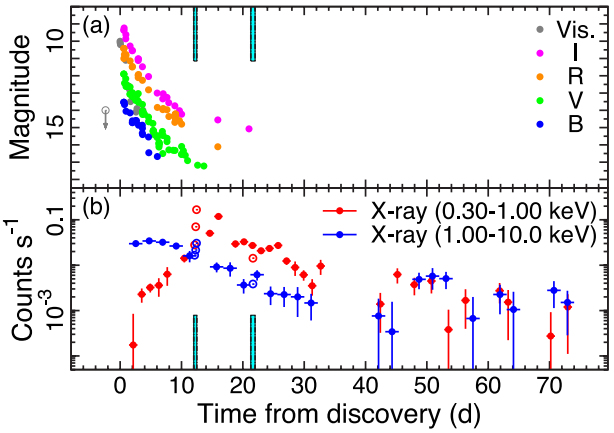

Fig. 1. Development of (a) optical and (b) X-ray brightness in the nova outburst of V2672 Oph. The origin of the abscissa in the modified Julian date is 55059.52 d, when the nova event was first discovered by Nakano, Yamaoka, and Kadota (2009b). The times of the Suzaku observations are indicated by the cyan regions. (a) *B*-, *V*-, *R*-, *I*-bands, and visual (i.e., non-filtered) magnitudes are shown color-coded. The upper-limit of the visual magnitude before the discovery of the nova is indicated by the open circle with the downward arrow. Optical data are from the American Association of Variable Star Observers (AAVSO), the Variable Star Observers League in Japan (VSOLJ), and telegrams by Nakano, Yamaoka, and Kadota (2009b); Nakano et al. (2009a); Nissinen et al. (2009); Ayani et al. (2009b); Munari et al. (2009). No ground-based photometry was taken after about day 20 as the optical brightness faded quickly. (b) Background-subtracted Swift/XRT count rates in the 0.3–1.0 keV and 1.0–10 keV energy bands are shown color-coded. Open circles indicate our time-averaged Suzaku results in each phase, which were converted into Swift/XRT count rates using the *pimms* software. The Swift observations were conducted by G. Schwarz on behalf of the Swift Nova-CV group (Schwarz et al. 2009, 2011).

R-band magnitude of 20.8 mag was found at the nova position in the Digitized Sky Survey images taken from 1991 to 1996 (Nakano et al. 2009a, 2009b), suggesting that the source suddenly brightened by more than $\sim$10 mag. The event was identified as a classical nova explosion, and was named Nova Ophiuchi 2009 and V2672 Ophiuchi (Nakano et al. 2009b).

Ground-based photometric and spectroscopic observations were subsequently conducted (Nakano et al. 2009a, 2009b; Nissinen et al. 2009; Ayani et al. 2009a, 2009b; Munari et al. 2009, 2011). Figure 1a shows the development of the nova brightness in optical and infrared wavelengths. Assuming the maximum *V*-band magnitude of 11.9 mag on 2009 August 17.134 UT (Nakano et al. 2009a), the decline rates t_2 and t_3 are $\sim$3 and 4 d, where t_2 and t_3 are the times to fade by 2 and 3 mag from its optical maximum, respectively; based on this, the nova type is classified as extremely fast. The $B-V$ color was estimated to be 1.81 mag on 2009 August 17.47 UT (Munari et al. 2009). An optical spectrum exhibited Hα, Hβ, O I, and possibly He I emission lines in the early phase (Munari et al. 2009). The velocity width of the Hα line was $\sim$8000 km s^{-1} on

day 1 (Ayani et al. 2009a). The rapid decline of its brightness and the extremely high velocity of ejecta suggest that the binary system comprises a massive white dwarf (Munari et al. 2009). The distance to V2672 Oph was estimated to be 19 ± 2 kpc based on the empirical relations of Downes and Duerbeck (2000); Cohen (1988); Schmidt (1957) using the optical data of Munari et al. (2011). In the radio regime, synchrotron emission with a flat spectral index ($\alpha \lesssim 1.2$) was detected on day 15.61 with the C configuration of the Very Large Array, suggesting that high-energy electrons were produced in shocked ejecta (Krauss Hartman et al. 2009).

2.2 Space-based observations

In the pre-outburst phase, no significant emission was found either in X-ray archival images taken by the ROSAT and ASCA satellites, or in the XMM-Newton slew survey (Schwarz et al. 2009). After the discovery, intensive monitoring observations were conducted by Swift and INTEGRAL (Schwarz et al. 2009, 2011). X-rays were first detected 1.43 d after the nova discovery using Swift, with a count rate of 0.017 s^{-1}. Ultraviolet emission was also detected with Swift, while no γ-ray emission was found with INTEGRAL 4 and 7 d after the discovery. Figure 1b shows the development of the Swift X-ray count rates. The turn-on and turn-off timescales of the supersoft phase were estimated to be 22 ± 2 and 28 ± 2 d, respectively, based on the Swift data (Schwarz et al. 2011). We requested target-of-opportunity observations with the Suzaku satellite to perform deep X-ray spectroscopy early in the evolution of V2672 Oph.

3 Observations and reduction

Target-of-opportunity observations of V2672 Oph were performed using the Suzaku X-ray observatory twice, on 2009 August 28 and September 6 (12 and 22 d after the discovery, respectively; see table 1). Suzaku has two X-ray instruments in operation (Mitsuda et al. 2007): the X-ray Imaging Spectrometer (XIS: Koyama et al. 2007) and the Hard X-ray Detector (HXD: Takahashi et al. 2007; Kokubun et al. 2007). In this paper, we concentrate on the XIS data in which significant X-ray emission from V2672 Oph was detected. The HXD signal was seriously contaminated by neighboring hard X-ray sources.

Table 1. Suzaku observations of V2672 Oph.

	Observation ID	
	904002010	904002020
t^*(d)	12.2	21.6
t_{start}[†](UT)	2009-08-28 12:20	2009-09-06 19:38
t_{end}[†](UT)	2009-08-29 00:00	2009-09-07 11:30
t_{exp}[‡](ks)	23.1	25.1

*Elapsed days in the middle of each observation from the discovery of V2672 Oph (55059.52 d in the modified Julian date).
†Start and end dates of the Suzaku observations.
‡Net exposure times averaged over the three operating CCDs.

The XIS is equipped with four X-ray CCDs at the foci of four co-aligned X-ray telescope modules (Serlemitsos et al. 2007). Three of them (XIS 0, 2, and 3) are front-illuminated (FI) CCDs sensitive in the 0.4–12 keV energy band, while the remaining one (XIS 1) is a back-illuminated (BI) CCD sensitive in the 0.2–12 keV range. Each chip has a format of 1024×1024 pixels, and covers an $\sim 18' \times 18'$ field of view. Two radioactive ^{55}Fe sources illuminate two corners of each CCD. Prior to the observation dates, XIS 2 and a part of XIS 0 became dysfunctional, and the data were excluded. The absolute energy scale is accurate to $\lesssim 10$ eV, and the full width at half maximum energy resolutions are ~ 180 and 230 eV at 5.9 keV for the FI and BI CCDs, respectively. The XIS was operated in the normal clocking mode with an 8 s frame time. The observations were aimed to put V2672 Oph at the center of the XIS field with almost the same roll angle in each.

Data were processed with the standard pipeline version 2.4,[1] in which events were removed during South Atlantic anomaly passages, when night-earth elevation angles were below 5°, and day-earth elevation angles were below 20°. The net exposure times were 23 and 25 ks on days 12 and 22, respectively. For data reduction and analysis, we used the High Energy Astrophysics software package version 6.7, the calibration database versions xis20090925 and xrt20080709, as well as the Sherpa fitting program (Freeman et al. 2001) in the Chandra Interactive Analysis of Observations package (Fruscione et al. 2006).

4 Analysis

4.1 Image analysis

Figure 2 shows smoothed XIS images in the 0.2–12.0 keV energy band on days 12 and 22. Events taken with each XIS were merged. The astrometry of the XIS images was registered by matching the position of V2672 Oph with that by an optical observation of Nakano, Yamaoka, and Kadota (2009b). For temporal and spectral analyses, source events were accumulated from a circular region with radii of 120 and 70 pixels (2.′1 and 1.′2) that were adaptively chosen to maximize the signal-to-noise ratio on days 12 and 22, respectively. Background events were accumulated from annular regions with inner and outer radii of 4′ and 7′ in each observation.

[1] See ⟨http://www.astro.isas.jaxa.jp/suzaku/process/⟩ for details.

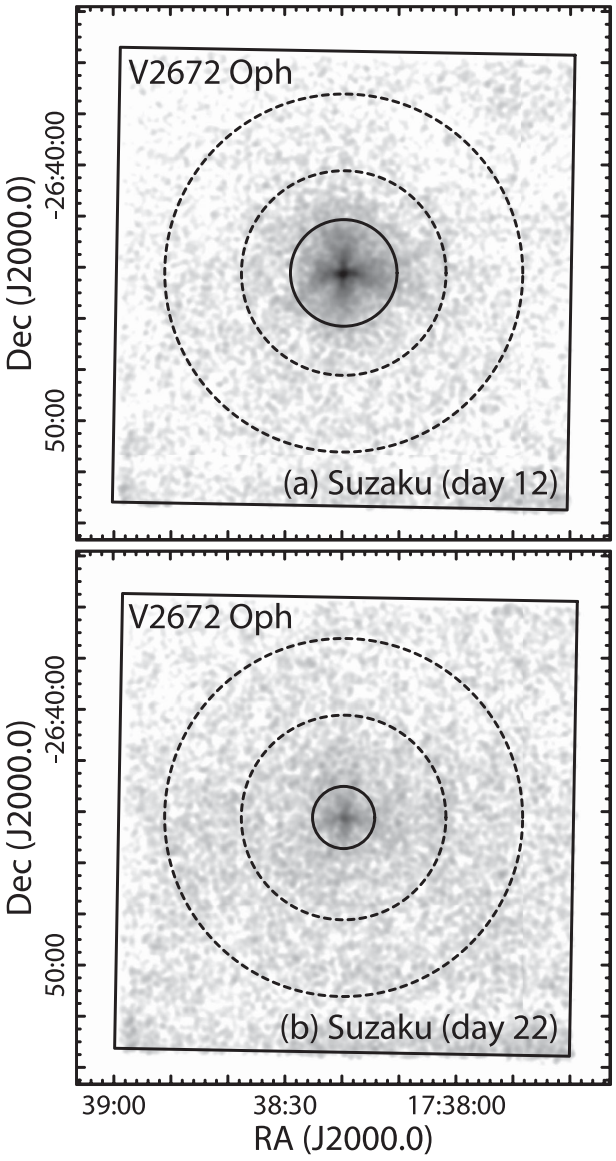

Fig. 2. Smoothed XIS images (a) 12 and (b) 22 d after the discovery. Events taken with the three CCDs in the 0.2–12.0 keV energy band were merged in each observation. The source and background extraction regions are indicated with the solid circles and the dashed annuli, respectively.

4.2 Temporal analysis

Figure 3 shows source and background light curves in the 0.2–12.0 keV energy band. On day 12, while the X-ray flux level had been stable in the first half of the observation, a prominent flux increase by a factor of nearly five was seen in the latter half. A significant correlation was found between the flux increase and the spectral softening on day 12 (figure 3). On day 22 the flux was relatively stable, showing variations, though at a much lower flux level. According to the flux development, we divided data on day 12 into three time slices (phases A–C), while data on day 22 are treated separately as phase D. The times defining each phase are as follows:

Phase A : day 12.0–12.3 (before the rise)
Phase B : day 12.3–12.4 (early in the rise)
Phase C : day 12.4–12.5 (later in the rise)
Phase D : day 21.3–22.0 (full data set on day 22).

For the sake of comparison, we further converted the time-averaged fluxes in each phase into Swift/XRT count rates by the *pimms* software (Mukai 1993). The long-term light curve including the Suzaku data (figure 1) shows a signature of large fluctuations below 1.0 keV at around day 12–16.

4.3 Spectral analysis

Figures 4 and 5 show background-subtracted XIS spectra of each time-slice. The two FI spectra with nearly identical responses were merged, while the BI spectra were treated separately for spectral analysis. The detector and mirror responses were generated by the `xisrmfgen` and `xissimarfgen` tools (Ishisaki et al. 2007), respectively.

The X-ray spectra are characterized by a soft excess below ~ 1 keV and a hard tail up to ~ 10 keV. On day 12 the soft component was highly variable, which corresponds to the flare-like brightening, while the hard component was relatively stable. Kα emission from Si XIII was clearly present and stronger than that from Si XIV. Prominent structures were found at both 0.6 and 0.9 keV, possibly by ionized absorption similar to those found in other novae (e.g., Ness et al. 2009b). In addition an unidentified structure was seen at 0.9–1.0 keV in phase C (the downward arrow in figure 4); this cannot be explained by Kα emission lines from highly ionized Ne assuming their rest energies. It also seems unlikely that either the Ne IX or Ne X emission lines are shifted by the Doppler effect with a velocity of $\gtrsim 10000\,\mathrm{km\,s^{-1}}$. One possible explanation might be a pseudo flux peak between prominent Ne IX and Ne X absorption lines, though no such structure has been reported in previous studies of novae. Then on day 22, both soft and hard components had faded significantly. Over time during this period, the dominant emission shifted toward lower energies.

4.3.1 Basic modeling

We first applied a combination of blackbody and optically-thin collisionally-ionized thermal plasma components to model softer and harder parts, respectively, of the V2672 Oph spectra. This approach has been used before for many other novae (e.g., Hernanz & Sala 2002; Ness et al. 2007a; Takei et al. 2008), and is driven by expectations of

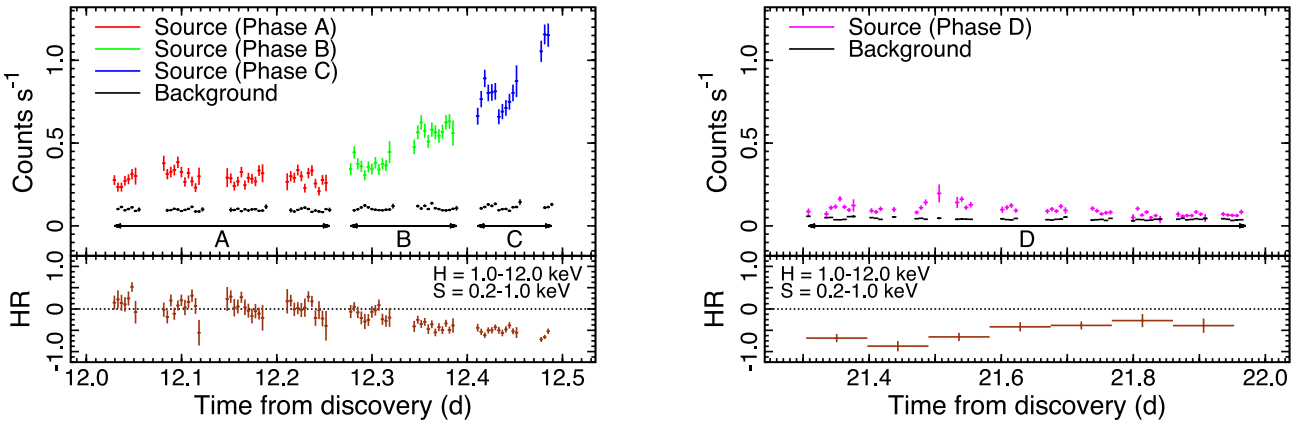

Fig. 3. The top panels show source and background XIS light curves on days 12 and 22. Events recorded by the three CCDs in the 0.2–12.0 keV energy band were merged. The source count rates are shown color-coded in each time-slice, and are labeled in terms of the behavioral phase (see text). The background count rates were normalized by the ratio of the extraction areas of the source and the background events. The normalized background count rates in the two observations are quite similar, and their difference is almost accounted for by the respective sizes of the source extraction regions. The bottom panels show hardness ratios (HRs) defined by $(H - S)/(H + S)$, where H and S are rates in the 0.2–1.0 keV and 1.0–12.0 keV energy bands, respectively. Data on day 22 were re-binned because of poor photon statistics.

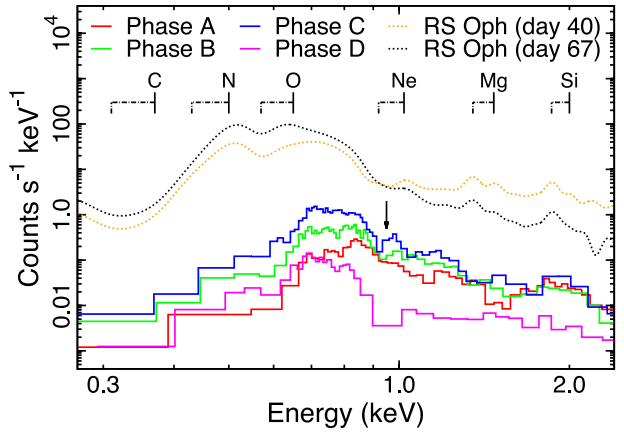

Fig. 4. Development of the X-ray spectra of V2672 Oph. The background-subtracted BI spectra are shown color-coded. The energies of plausible Kα emission lines are labeled with solid- and dashed-lines for H- and He-like ions, respectively. The downward arrow indicates the unidentified structure described in subsection 4.3. For comparison, the dashed curves are X-ray spectra of RS Oph 2006 taken by the Chandra grating instruments 40 and 67 d after the outburst, convolved with the Suzaku XIS-BI response.

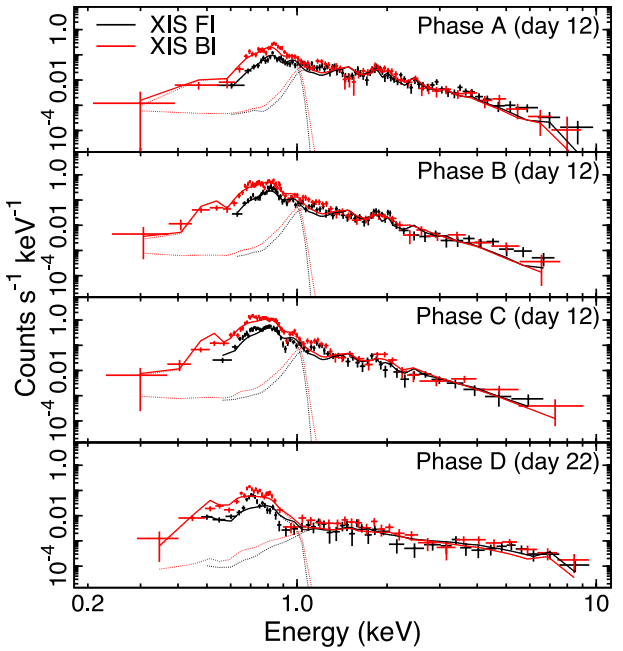

Fig. 5. Background-subtracted XIS spectra and the best-fit models using the normalized supersoft component of RS Oph 2006 taken on day 67 and the MEKAL plasma code convolved with photoelectric absorption. The best-fit models are shown by solid lines, while each component is illustrated by dashed lines.

optically-thin emission from expanding ejecta and optically-thick photospheric emission from the supersoft source. The MEKAL code (Mewe et al. 1985) was adopted to represent the optically-thin plasma emission, and the elemental abundances for this were fixed to be solar. Both emission components were multiplied with an interstellar absorption model (TBabs: Wilms et al. 2000). The free parameters in the combined model were a hydrogen-equivalent column density ($N_{\rm H}$), blackbody temperature ($k_{\rm B}T_{\rm BB}$) and bolometric luminosity ($L_{\rm BB}$), and MEKAL plasma temperature ($k_{\rm B}T_{\rm TH}$) and X-ray volume emission measure (EM). We also calculated X-ray fluxes ($F_{\rm SX}$ and $F_{\rm HX}$) and absorption-corrected luminosities ($L_{\rm SX}$ and $L_{\rm HX}$) in softer and harder (0.2–1.0 and 1.0–10 keV) energy bands, respectively. For the luminosity estimates, the distance to V2672 Oph was assumed to be 19 kpc (Munari et al. 2011). The best-fit parameters producing the minima in the Xspec version of the χ^2 statistics with data variance are summarized in table 2. This basic model provides a good representation of the data above $\sim$1 keV, while significant residuals were found in

Table 2. Best-fit parameters of the X-ray spectra of V2672 Oph.

Component	Parameter	Units	Phase A*	Phase B*	Phase C*	Phase D*
TBabs × (Blackbody + MEKAL) (sub-subsection 4.3.1)						
Absorption	$N_{\rm H}$	(10^{22} cm^{-2})	$2.08^{+0.16}_{-0.15}$	$1.61^{+0.14}_{-0.27}$	$1.59^{+0.15}_{-0.15}$	$0.69^{+0.17}_{-0.15}$
Blackbody	$k_{\rm B}T_{\rm BB}$	(eV)	$44.3^{+2.48}_{-2.24}$	$48.8^{+5.75}_{-2.57}$	$47.7^{+3.97}_{-2.64}$	$60.8^{+5.99}_{-5.38}$
	$L_{\rm BB}$§	(10^{40} erg s^{-1})	$104.8^{+276.0}_{-69.8}$	$10.0^{+21.8}_{-6.95}$	$24.1^{+71.2}_{-17.8}$	$0.003^{+0.013}_{-0.002}$
Plasma	$k_{\rm B}T_{\rm TH}$	(keV)	$0.97^{+0.08}_{-0.07}$	$1.02^{+0.36}_{-0.11}$	$1.00^{+0.33}_{-0.16}$	$5.04^{+6.28}_{-1.64}$
	EM§	(10^{57} cm^{-3})	$12.7^{+1.00}_{-1.82}$	$8.97^{+1.75}_{-2.78}$	$10.5^{+2.92}_{-2.87}$	$0.79^{+0.16}_{-0.13}$
Flux	$F_{\rm SX}$†	(10^{-12} erg s^{-1} cm^{-2})	$0.55^{+0.03}_{-0.55}$	$1.45^{+0.08}_{-1.45}$	$2.87^{+0.04}_{-2.85}$	$0.38^{+0.07}_{-0.38}$
	$F_{\rm HX}$‡	(10^{-12} erg s^{-1} cm^{-2})	$0.62^{+0.03}_{-0.11}$	$0.67^{+0.03}_{-0.18}$	$0.83^{+0.04}_{-0.26}$	$0.24^{+0.03}_{-0.06}$
Luminosity	$L_{\rm SX}$†§	(10^{40} erg s^{-1})	∼30.2	∼3.39	∼8.86	∼0.002
	$L_{\rm HX}$‡§	(10^{35} erg s^{-1})	$4.65^{+0.21}_{-0.83}$	$2.87^{+0.14}_{-0.77}$	$4.22^{+0.19}_{-1.30}$	$0.14^{+0.02}_{-0.03}$
χ^2/d.o.f.			239/144	429/138	893/129	522/92
TBabs × (Blackbody + MEKAL) (sub-subsection 4.3.1, for comparison)						
Absorption	$N_{\rm H}$	(10^{22} cm^{-2})		— $1.71^{+0.08}_{-0.10}$ —		—
Blackbody	$k_{\rm B}T_{\rm BB}$	(eV)	$50.9^{+2.24}_{-1.73}$	$47.0^{+1.86}_{-1.44}$	$45.6^{+1.77}_{-1.35}$	—
	$L_{\rm BB}$§	(10^{40} erg s^{-1})	$3.81^{+4.14}_{-2.24}$	$25.0^{+27.1}_{-14.7}$	$71.1^{+78.4}_{-42.2}$	—
Plasma	$k_{\rm B}T_{\rm TH}$	(keV)	$1.25^{+0.11}_{-0.09}$	$0.99^{+0.12}_{-0.11}$	$0.96^{+0.13}_{-0.18}$	—
	EM§	(10^{57} cm^{-3})	$8.16^{+0.79}_{-0.89}$	$9.89^{+1.43}_{-1.52}$	$11.9^{+3.73}_{-1.99}$	—
χ^2/d.o.f.				— 1579/413 —		—
Absorption	$N_{\rm H}$	(10^{22} cm^{-2})	$1.92^{+0.09}_{-0.10}$	$1.70^{+0.08}_{-0.09}$	$1.63^{+0.08}_{-0.09}$	—
Blackbody	$k_{\rm B}T_{\rm BB}$	(eV)		— $46.9^{+1.65}_{-1.37}$ —		—
	$L_{\rm BB}$§	(10^{40} erg s^{-1})	$25.8^{+28.4}_{-14.6}$	$25.5^{+27.5}_{-14.3}$	$35.1^{+37.2}_{-19.5}$	—
Plasma	$k_{\rm B}T_{\rm TH}$	(keV)	$1.00^{+0.09}_{-0.07}$	$0.99^{+0.11}_{-0.12}$	$0.99^{+0.13}_{-0.15}$	—
	EM§	(10^{57} cm^{-3})	$11.2^{+1.38}_{-1.41}$	$9.92^{+1.43}_{-1.46}$	$11.0^{+1.79}_{-1.83}$	—
χ^2/d.o.f.				— 1565/413 —		—
Absorption	$N_{\rm H}$	(10^{22} cm^{-2})	$1.93^{+0.09}_{-0.09}$	$1.72^{+0.08}_{-0.09}$	$1.60^{+0.08}_{-0.09}$	—
Blackbody	$k_{\rm B}T_{\rm BB}$	(eV)	$46.7^{+1.62}_{-1.39}$	$46.8^{+1.63}_{-1.40}$	$47.4^{+1.69}_{-1.44}$	—
	$L_{\rm BB}$§	(10^{40} erg s^{-1})		— $27.7^{+30.2}_{-15.3}$ —		—
Plasma	$k_{\rm B}T_{\rm TH}$	(keV)	$1.00^{+0.09}_{-0.07}$	$0.98^{+0.11}_{-0.13}$	$1.00^{+0.14}_{-0.14}$	—
	EM§	(10^{57} cm^{-3})	$11.3^{+1.38}_{-1.39}$	$10.0^{+1.46}_{-1.46}$	$10.7^{+1.79}_{-1.81}$	—
χ^2/d.o.f.				— 1565/413 —		—
TBabs × (NLTE Atmosphere + MEKAL) (sub-subsection 4.3.2)						
Absorption	$N_{\rm H}$	(10^{22} cm^{-2})	$2.17^{+0.05}_{-0.05}$	$1.90^{+0.04}_{-0.05}$	$1.75^{+0.04}_{-0.04}$	$1.46^{+0.04}_{-0.07}$
Atmosphere	$k_{\rm B}T_{\rm NL}$	(eV)	$69.1^{+0.04}_{-0.03}$	$69.1^{+0.04}_{-0.03}$	$69.1^{+0.04}_{-0.03}$	$68.9^{+0.04}_{-1.61}$
	$N_{\rm NL}$‖	(10^{-3})	$1.99^{+0.55}_{-0.48}$	$1.71^{+0.47}_{-0.41}$	$1.91^{+0.49}_{-0.43}$	$0.08^{+0.02}_{-0.03}$
Plasma	$k_{\rm B}T_{\rm TH}$	(keV)	$1.03^{+0.17}_{-0.08}$	$1.01^{+0.13}_{-0.10}$	$1.02^{+0.22}_{-0.11}$	$3.33^{+4.63}_{-1.58}$
	EM§	(10^{57} cm^{-3})	$11.6^{+1.36}_{-1.35}$	$9.82^{+1.44}_{-1.44}$	$10.4^{+1.75}_{-1.94}$	$1.11^{+0.22}_{-0.21}$
Flux	$F_{\rm SX}$†	(10^{-12} erg s^{-1} cm^{-2})	$0.56^{+0.04}_{-0.06}$	$1.68^{+0.09}_{-0.15}$	$3.91^{+0.16}_{-0.30}$	$0.52^{+0.03}_{-0.06}$
	$F_{\rm HX}$‡	(10^{-12} erg s^{-1} cm^{-2})	$0.65^{+0.04}_{-0.05}$	$0.68^{+0.04}_{-0.05}$	$0.85^{+0.06}_{-0.08}$	$0.22^{+0.03}_{-0.04}$
Luminosity	$L_{\rm SX}$†§	(10^{40} erg s^{-1})	∼4.68	∼4.01	∼4.51	∼0.18
	$L_{\rm HX}$‡§	(10^{35} erg s^{-1})	$5.68^{+0.32}_{-0.40}$	$4.91^{+0.32}_{-0.40}$	$5.60^{+0.39}_{-0.51}$	$0.26^{+0.03}_{-0.05}$
χ^2/d.o.f.			194/144	197/138	346/129	282/92

Table 2. (Continued.)

Component	Parameter	Units	Phase A*	Phase B*	Phase C*	Phase D*
phabs × (Unfolded RS Oph 2006 + MEKAL) (sub-subsection 4.3.3)						
Absorption	$N_{\rm H}$	(10^{22} cm^{-2})	$1.22^{+0.06}_{-0.06}$	$0.92^{+0.04}_{-0.04}$	$0.82^{+0.03}_{-0.03}$	$0.38^{+0.04}_{-0.04}$
RS Oph 2006	$A_{\rm RS}$	(RS Oph 2006 on day 67)	$0.87^{+0.26}_{-0.20}$	$0.63^{+0.12}_{-0.10}$	$0.90^{+0.13}_{-0.11}$	$0.010^{+0.003}_{-0.002}$
Plasma	$k_{\rm B}T_{\rm TH}$	(keV)	$1.24^{+0.08}_{-0.21}$	$1.22^{+0.09}_{-0.11}$	$1.30^{+0.12}_{-0.12}$	$4.91^{+2.67}_{-1.37}$
	EM[§]	(10^{57} cm^{-3})	$6.82^{+0.90}_{-0.49}$	$6.02^{+0.44}_{-0.43}$	$6.70^{+0.53}_{-0.52}$	$0.74^{+0.10}_{-0.09}$
Flux	$F_{\rm SX}$[†]	(10^{-12} erg s^{-1} cm^{-2})	$0.59^{+0.18}_{-0.14}$	$1.74^{+0.34}_{-0.29}$	$4.03^{+0.57}_{-0.51}$	$0.52^{+0.13}_{-0.11}$
	$F_{\rm HX}$[‡]	(10^{-12} erg s^{-1} cm^{-2})	$0.60^{+0.08}_{-0.04}$	$0.64^{+0.05}_{-0.05}$	$0.78^{+0.06}_{-0.06}$	$0.23^{+0.03}_{-0.03}$
Luminosity	$L_{\rm SX}$[†§#]	(10^{37} erg s^{-1})	>1.16	>0.90	>1.36	>0.01
	$L_{\rm HX}$[‡§]	(10^{35} erg s^{-1})	$0.49^{+0.07}_{-0.04}$	$0.43^{+0.03}_{-0.03}$	$0.48^{+0.04}_{-0.04}$	$0.070^{+0.009}_{-0.008}$
χ^2/d.o.f.			265/145	252/139	417/130	289/93

* Statistical uncertainties indicate the 90% confidence ranges in the Xspec version of the χ^2 statistics.
† Values are in the 0.2–1.0 keV energy band.
‡ Values are in the 1.0–10 keV energy band.
§ Values are for a distance of 19 kpc (Munari et al. 2011).
# Values are the normalization of astrophysical fluxes at a distance of 1 pc.
‖ Values are lower limits because of the additional unresolved absorption in the RS Oph 2006 component.

the softer part of the spectrum, particularly near 0.6, 0.9, and 0.9–1.0 keV, where we infer the presence of significant additional local structures.

Based on the basic modeling, we then measured χ^2 increases with an additional null hypothesis that either $N_{\rm H}$, $k_{\rm B}T_{\rm BB}$, or $L_{\rm BB}$ was constant during the rapid flux rise in phases A–C. The best-fit values for comparison are also summarized in table 2. The resulting χ^2 values and the degrees of freedom indicate that the F-test statistics for changing $N_{\rm H}$, $k_{\rm B}T_{\rm BB}$, or $L_{\rm BB}$ are 2.48, 0.63, and 0.60, which can be converted to F-test null hypothesis probabilities of 0.09, 0.53, and 0.55, respectively. Even though these statistical tests are not strictly accurate in our case because of non-normality (see e.g., Orlandini et al. 2012), it seems likely that the time development in phases A–C would be subject to a change in absorption.

We emphasize here that the blackbody approximation is only suitable as a first-order description of the underlying spectrum, and the best-fit effective temperature and luminosity can differ greatly from actual values, whether the spectral shape is well-fitted or not (e.g., Krautter et al. 1996; Takei & Ness 2010). This is because nova supersoft X-ray spectra result from radiative transfer within an expanding medium, and exhibit numerous complex absorption features, often combined with emission lines (e.g., Ness et al. 2007b, 2009b, 2012). While it might be possible to obtain a statistically more acceptable fit from adding further local components to the model, the exercise would be arbitrary in the context of attempting to learn more about the emitting source. In the following subsections we focus on the softer part, and adopt more sophisticated spectral models in the place of the blackbody component.

4.3.2 Atmosphere modeling

As the second fitting approach, we applied a Non-Local Thermodynamic Equilibrium (NLTE) atmospheric model (Tübingen NLTE Model-Atmosphere Fluxes: e.g., Rauch 1997), instead of a blackbody model for the soft component. The theoretical spectral energy distributions were calculated for elements H–Ca with solar abundances, and approximated formulae were employed to treat any Stark line-broadening (Rauch 1993). Assuming a massive white dwarf close to the Chandrasekhar limit (e.g., Munari et al. 2009), we adopted a logarithmic surface gravity of $\log g = 9$. The effective temperature ($k_{\rm B}T_{\rm NL}$) and a normalization parameter of the model flux ($N_{\rm NL}$) were treated as free parameters. The best-fit results are also summarized in table 2. The use of these atmospheric models slightly improved the goodness of fit, in comparison to that of the basic blackbody model.

4.3.3 Comparison with RS Ophiuchi 2006

To go one step further with spectroscopy, we compared the X-ray spectra of V2672 Oph with those of RS Oph 2006, which is one of only a handful of novae for which detailed multi-wavelength data sets including X-rays have been obtained to date. X-ray grating spectra of the supersoft emission in RS Oph 2006 were obtained at three different epochs [days 54 (XMM-Newton), 40 and 67 (Chandra):

e.g., Ness et al. 2009b]. In order to compare the medium-resolution V2672 Oph CCD spectra with high-resolution grating data for RS Oph 2006, we first calculated the photon flux spectra using the instrumental responses of each grating observation. The resulting spectra were then convolved with the XIS responses, assuming that instrumental line broadening of the grating spectra is negligible; the resolving power is more than 10 times higher than that of the CCD spectrometers. Figure 4 shows these resultant degraded grating spectra of RS Oph 2006, which were obtained in the supersoft X-ray phase, 40 and 67 d after the outburst using Chandra. We here focus on the Chandra data set because the X-ray spectra at the two different epochs were obtained by the same instrument. The spectral development of V2672 Oph is basically analogous to that of RS Oph 2006, in which the peak energy of the supersoft component shifts toward lower energies as time progresses (see figure 4). The heavy attenuation at 0.9 keV, which we attributed to atmospheric absorption, is also similar to a pattern seen in RS Oph 2006 spectra (see also figure 4).

We fitted the V2672 Oph spectra by a combination of the MEKAL plasma component and the unfolded RS Oph 2006 spectrum, convolved with a photoelectric absorption (phabs in Xspec). Grating data in the 0.2–1.0 keV energy band that were dominated by supersoft emission with negligible contribution ($\lesssim 1\%$) of the plasma component of RS Oph 2006 were used for fitting. The normalization of the RS Oph 2006 component ($A_{\rm RS}$) was treated as a free parameter. Elemental abundances for the photoelectric absorption model were fixed to be solar. We compared the goodness of fit in each phase using Chandra data at the two different epochs. Empirically, the day 67 model provides the best fits in all phases. The best-fit results are listed in table 2 and are shown in figure 5.

5 Discussion

5.1 Supersoft emission

The supersoft component is similar in character to that of other novae, and so the origin can be considered to be photospheric emission powered by post-outburst residual nuclear burning on the white dwarf. The long-term supersoft X-ray rise clearly coincides with the optical decline until about day 15 (figure 1), suggesting that the dominant emission shifted toward higher energies as the mass outflow diminished, and consequently the photon escape region was formed deeper in the ejected material. The temperatures of 40–70 eV are also typical of those found in other supersoft sources and novae (e.g., Greiner 2000). Then, the supersoft emission faded out on day 22, suggesting that the nuclear burning rate was reduced on the white-dwarf surface.

It has to be noted that an actual X-ray luminosity is difficult to estimate because of large spectral model-dependent systematic uncertainties in the supersoft emission. Also, the distance estimate of 19 kpc is subject to uncertainties (Munari et al. 2011). The blackbody and NLTE atmosphere luminosity estimates are almost certainly too high because they exceed the Eddington limit of a Chandrasekhar white dwarf, while the RS Oph 2006 values are underestimated as the model itself contains intrinsic absorption. Within the large uncertainty from the three model approaches we chose as a working hypothesis the values of the luminosity of the NLTE atmosphere model. The values at 19 kpc are 10^{39}–$10^{40}\,{\rm erg\,s^{-1}}$ in the 0.2–1.0 keV energy band. The softer band luminosity estimates clearly exceed the Eddington values.

The rapid flux rise on day 12 is consistent with a model in which the intrinsic absorption of the nova outburst declined with time. This is because the absorption dropped with increasing supersoft X-ray intensity (table 2). In addition, the hydrogen-equivalent absorption column densities on day 12 significantly exceeded the interstellar Galactic value of $3.8 \times 10^{21}\,{\rm cm^{-2}}$, which is from H I intensity maps (Kalberla et al. 2005) for a 1° cone radius at the V2672 Oph position, and can be considered to be an upper limit. The *F*-test results might further support this scenario. This suggests that the supersoft emission would be affected by the time development of surrounding ejecta.

In contrast to the absorber, no significant growth can be otherwise confirmed in the emission components during the rapid flux rise on day 12. This indicates that the broad-band fitting of the limited CCD data does not allow us to examine whether the supersoft component contributed to the spectral changes simultaneously. We here cannot exclude a scenario that the time development of emission lines like those of RS Oph 2006 (e.g., Nelson et al. 2008; Ness et al. 2009b) contributes to the spectral changes. Further, the nature of unidentified structure at 0.9–1.0 keV in phase C is still an open question. Higher-resolution spectroscopy would have been required to provide a reliable diagnostic of the time development of the emission components.

Assuming that the intrinsic absorption contributed to the rapid flux rise on day 12, the decline rate of the column densities poses a challenge to understanding the time development of the mass outflow. For example, assuming spherically symmetric ejecta with a gradient density distribution, the gas density profile is

$$\rho \sim \frac{1}{4\pi r^2}\frac{\dot{M}}{v}, \tag{1}$$

where r is a radial distance, v is an ejecta velocity, and $\dot{M}$ is a time-dependent mass-loss rate. The intrinsic absorption

can be approximated by

$$N_{\rm H} \sim \int_{r_{\rm wd}}^{r_{\rm out}} \rho dr \sim \frac{\dot{M}}{4\pi v r_{\rm wd}} \left(1 - \frac{r_{\rm wd}}{r_{\rm out}}\right), \quad (2)$$

where $r_{\rm wd}$ is a white-dwarf radius and $r_{\rm out}$ is the outermost radius of ejecta. Assuming that the time scale of the terminal velocity decline is much larger than the time for the ejecta to reach the outermost radius, $r_{\rm out} \approx vt$ at time t. By adopting a constant velocity, while assuming an initial free expansion stage, $r_{\rm out} \gg r_{\rm wd}$ and the intrinsic absorption decreases only in proportion to the decrease in $\dot{M}$. A time-dependent mass-loss rate can be further assumed as (e.g., Bode & Evans 2008; Takei et al. 2013),

$$\dot{M} = \dot{M}_0 (t_0/t)^p, \quad (3)$$

where $\dot{M}_0$ is an initial value normalized at time $t = t_0 = 1$ s and p is a measure of the speed of its decline. This indicates that we can make a crude estimate of p from the decline rate of the observed column densities.

The difference in the absorption column densities between days 12 and 22 is (0.6–1.7) $\times$ 10^{22} cm^{-2}, which corresponds to a decline rate of about 30%–80% on a time scale of 10 d. This does not depend on the fitting models, and is much too fast to be explained by a thinning of uniform ejecta, even assuming a non-decelerated expansion velocity. Based on the result, a measure of the decline rate given by equation (3) is $p \sim 0.6$–2.7, suggesting that the long-term $\dot{M}$ decline time scale is similar to that derived from U Sco 2010 (Takei et al. 2013). The value is also consistent with a prediction that p is of order unity (e.g., Bode & Evans 2008). In contrast, the difference in the short-term column densities between phases A and C on day 12 is (2–8) $\times$ 10^{21} cm^{-2}, and its decline rate is about 10%–40% on a time scale of 0.2 d relative to the phase A values. This can be converted to $p \sim 6.3$–31, according to equation (3). Though we cannot exclude a scenario that the reality has more complex trends of $\dot{M}$, the values indicate that the cause of the rapid rise on day 12 cannot reasonably be explained by the same framework of the long-term development.

We finally expect that the rapid absorption drop on day 12 and the subsequent large fluctuations (figure 1) are likely to betray a non-uniform density distribution of the ejected material [e.g., see figure 2 in Shaviv and Dotan (2010) and figure 5 in Williams (2013)]. Less-dense regions of the ejecta would be preferentially broken by the strong radiation pressure, particularly since the photospheric emission is close to the Eddington luminosity (e.g., Owocki et al. 1988; Shaviv & Dotan 2010). The surrounding material would be porous and clumpy, and full of holes, like Swiss cheese. The relatively stable light curve in phase A can be interpreted as the presence of a dense blob or thin hole in the line of sight, while the flux rise in phases B–C results from the hole expanding, or the blob gradually moving out of the line of sight.

5.2 Optically-thin thermal plasma emission

The Swift light curve in the harder energy band exhibits a continuous flux decline, except for a brightening around day 50, since its eruption (figure 1), indicating that the origin of the harder component is different from that of the supersoft component. This is similar to the findings from previous nova explosions (e.g., Tsujimoto et al. 2009). The temperature of this component is several keV, indicating an origin in shock-excited plasma resulting from kinematic interactions within the outflow (e.g., Mukai & Ishida 2001). The harder band estimates are typical of those derived for other novae (e.g., Tsujimoto et al. 2009). The difference of the plasma temperatures in phases A–C and D might, in principle, be of interest for constraining a heating mechanism, though the values have large uncertainties because of the poor photon statistics and the high background levels in the higher energy band.

6 Summary

We conducted target-of-opportunity observations of the classical nova V2672 Ophiuchi, 12 and 22 d after its discovery, using the Suzaku X-ray satellite. The X-ray light curve exhibited a clear flux amplification on day 12; then, the fluxes became significantly smaller on day 22. X-ray spectra were modeled by a supersoft source and an optically-thin thermal plasma component convolved with a photoelectric absorption model. The spectral evolution of the X-ray rise can be accounted for by a reduction in the absorption over time, with a decline of 10%–40% on a time scale of 0.2 d. This rapid drop of absorption and the associated short-term variability on day 12 indicate inhomogeneous and porous ejecta, with dense blobs or holes in the line-of-sight.

Acknowledgments

The authors appreciate the reviewer for useful suggestions. We thank the Suzaku telescope managers for allocating a part of the director's discretionary time, and also thank Greg Schwarz, the principal investigator of the Swift observations, and the Nova-CV group for providing the Swift data. Optical data are from AAVSO and VSOLJ databases. This research has made use of data obtained from: (1) DARTS by C-SODA in JAXA/ISAS, (2) HEASARC by NASA/GSFC, and (3) SIMBAD by CDS, France. We acknowledge

Jan-Uwe Ness for his comments on this paper. D. T. acknowledges financial support from JSPS and by the Special Postdoctoral Researchers Program in RIKEN. J. J. D. was supported by the NASA contract NAS8-03060 to the CXC and thanks the Director, H. Tananbaum, for continuing advice and support.

References

Ayani, K., et al. 2009b, IAU Circ., 9064
Ayani, K., Murakami, N., Hata, K., Tanaka, A., Tachibana, M., & Kanda, A. 2009a, Cent. Bur. Electron. Telegrams, 1911, 1
Beardmore, A. P., et al. 2010a, Astronomer's Telegram, 2423
Beardmore, A. P., et al. 2010b, Astrono. Nachr., 331, 156
Bode, M. F., et al. 2009, Astronomer's Telegram, 2025
Bode, M. F., & Evans, A. 2008, Classical Novae, 2nd ed. (New York: Cambridge University Press)
Cohen, J. G. 1988, in ASP Conf. Ser., 4, The Extragalactic Distance Scale, ed. S. van den Bergh & C. J. Pritchet (San Francisco: ASP), 114
Downes, R. A., & Duerbeck, H. W. 2000, AJ, 120, 2007
Drake, J. J., et al. 2003, ApJ, 584, 448
Freeman, P. E., Doe, S., & Siemiginowska, A. 2001, in Proc. SPIE, 4477, Astronomical Data Analysis, ed. J.-L. Starck & F. D. Murtagh (Bellingham, WA: SPIE), 76
Fruscione, A., et al. 2006, in Proc. SPIE, 6270, Observatory Operations: Strategies, Processes, and Systems, ed. D. R. Silva & R. E. Doxsey (Bellingham, WA: SPIE), 62701v
Greiner, J. 2000, New Astron., 5, 137
Hernanz, M., & Sala, G. 2002, Science, 298, 393
Ishisaki, Y., et al. 2007, PASJ, 59, S113
Kalberla, P. M. W., Burton, W. B., Hartmann, D., Arnal, E. M., Bajaja, E., Morras, R., & Pöppel, W. G. L. 2005, A&A, 440, 775
Kokubun, M., et al. 2007, PASJ, 59, S53
Koyama, K., et al. 2007, PASJ, 59, S23
Krauss Hartman, M. I., Rupen, M. P., & Mioduszewski, A. J. 2009, Astronomer's Telegram, 2195
Krautter, J., Ögelman, H., Starrfield, S., Wichmann, R., & Pfeffermann, E. 1996, ApJ, 456, 788
Mewe, R., Gronenschild, E. H. B. M., & van den Oord, G. H. J. 1985, A&AS, 62, 197
Mitsuda, K., et al. 2007, PASJ, 59, S1
Mukai, K. 1993, Legacy, 3, 21
Mukai, K., & Ishida, M. 2001, ApJ, 551, 1024
Munari, U., Ribeiro, V. A. R. M., Bode, M. F., & Saguner, T. 2011, MNRAS, 410, 525
Munari, U., Saguner, T., Ochner, P., Siviero, A., Maitan, A., Valisa, P., Dallaporta, S., & Moretti, S. 2009, Cent. Bur. Electron. Telegrams, 1912, 1
Nakano, S., Yamaoka, H., Itagaki, K., et al. 2009a, IAU Circ. 9064, 1
Nakano, S., Yamaoka, H., & Kadota, K. 2009b, Central Bureau Electronic Telegrams, 1910, 1
Nelson, T., Orio, M., Cassinelli, J. P., Still, M., Leibowitz, E., & Mucciarelli, P. 2008, ApJ, 673, 1067
Ness, J.-U., et al. 2003, ApJ, 594, L127
Ness, J.-U., et al. 2007b, ApJ, 665, 1334
Ness, J.-U., et al. 2009a, AJ, 137, 4160
Ness, J.-U., et al. 2009b, AJ, 137, 3414
Ness, J.-U., et al. 2012, ApJ, 745, 43
Ness, J.-U., Schwarz, G. J., Retter, A., Starrfield, S., Schmitt, J. H. M. M., Gehrels, N., Barrows, D., & Osborne, J. P. 2007a, ApJ, 663, 505
Nissinen, M., Hentunen, V., Kiyota, S., & Elenin, L. 2009, Cent. Bur. Electron. Telegrams, 1910, 2
Orlandini, M., Frontera, F., Masetti, N., Sguera, V., & Sidoli, L. 2012, ApJ, 748, 86
Osborne, J. P., et al. 2011, ApJ, 727, 124
Owocki, S. P., Castor, J. I., & Rybicki, G. B. 1988, ApJ, 335, 914
Rauch, T. 1993, A&A, 276, 171
Rauch, T. 1997, A&A, 320, 237
Schmidt, T. 1957, Z. Astrophys., 41, 182
Schwarz, G. J., et al. 2009, Astronomer's Telegram, 2173
Schwarz, G. J., et al. 2011, ApJS, 197, 31
Serlemitsos, P. J., et al. 2007, PASJ, 59, S9
Shaviv, N. J., & Dotan, C. 2010, Mem. Soc. Astron. Ital., 81, 350
Starrfield, J. H., Illiadis, C., & Hix, W. R. 2008, in Classical Novae, ed. Bode, M., & Evans, A. (Cambridge: Cambridge University Press), 77
Takahashi, T., et al. 2007, PASJ, 59, S35
Takei, D., Drake, J. J., Tsujimoto, M., Ness, J.-U., Osborne, J. P., Starrfield, S., & Kitamoto, S. 2013, ApJ, 769, L4
Takei, D., & Ness, J.-U. 2010, Astrono. Nachr., 331, 183
Takei, D., Tsujimoto, M., Kitamoto, S., Morii, M., Ebisawa, K., Maeda, Y., & Miller, E. D. 2008, PASJ, 60, S231
Tsujimoto, M., Takei, D., Drake, J. J., Ness, J., & Kitamoto, S. 2009, PASJ, 61, S69
Warner, B. 2003, Cataclysmic Variable Stars (Cambridge: Cambridge University Press)
Williams, R. 2013, AJ, 146, 55
Wilms, J., Allen, A., & McCray, R. 2000, ApJ, 542, 914